RADIO SCIENCE, VOL. 41, RS2S14, doi:10.1029/2005RS003402, 2006

Three-dimensional finite difference time domain modeling of the diurnal and seasonal variations in Schumann resonance parameters

Heng Yang[1] and Victor P. Pasko[1]

Received 3 October 2005; revised 27 January 2006; accepted 22 March 2006; published 21 October 2006.

[1] The diurnal and seasonal variations of Schumann resonances (SR) have been reported in a number of experiments. In this paper, a three-dimensional FDTD model of the Earth-ionosphere cavity with a day-night asymmetric conductivity profile is employed to study the diurnal and seasonal variability of the power and frequency of the first Schumann resonance (SR) mode. Comparison of the FDTD results and recent experimental measurements shows a clear modulation in the SR power related to the local ionospheric height and global lightning activity. It is found that SR frequencies are not only a function of the local time but also are controlled by the global lightning activity changing with universal time.

Citation: Yang, H., and V. P. Pasko (2006), Three-dimensional finite difference time domain modeling of the diurnal and seasonal variations in Schumann resonance parameters, *Radio Sci.*, *41*, RS2S14, doi:10.1029/2005RS003402 [Printed *42*(2), 2007].

1. Introduction

[2] The combination of the highly conducting terrestrial surface boundary and the highly conducting ionospheric boundary separated by a weakly conducting atmosphere creates a spherically concentric cavity, the Earth-ionosphere cavity. The electromagnetic waves produced by global lightning activity are trapped in this cavity. Because of the conduction losses in the cavity, only electromagnetic signals below 100 Hz can propagate long distances without suffering serious attenuation, and the interference between the waves travelling in multiple paths produces global resonances [*Sentman*, 1995; *Nickolaenko and Hayakawa*, 2002]. *Schumann* [1952] first predicted the resonance properties of this cavity, so these resonances are commonly referred to as Schumann resonances (SR). Because the SR parameters (e.g., power, frequency, and Q factor) are mainly determined by the global lightning activity and the electromagnetic properties of the lower ionosphere, observations of SR have been used in many remote sensing applications [e.g., *Williams*, 1992; *Cummer*, 2000; *Shvets*, 2001].

[3] The SR parameters are sensitive to the external perturbations. During the solar proton events (SPE), high-energy particle precipitation is often accompanied by X-ray bursts leading to significant perturbations of the conductivity in the cavity. Different shifts of the SR parameters were reported in the realistic measurements [e.g., *Schlegel and Füllekrug*, 1999; *Roldugin et al.*, 2001, 2003, 2004a; *Sátori et al.*, 2005]. In our previous work [*Yang and Pasko*, 2005], the variation patterns of the first SR frequency associated with the ionospheric conductivity perturbation during SPEs and X-ray bursts were discussed. It has been demonstrated that the conductivity perturbation at high altitudes (>70 km) leads to increase in the first SR frequency; whereas, the first SR frequency decreases with the conductivity perturbation at low altitudes (<70 km).

[4] Besides the SR parameter shifts during the high-energy particle precipitation and X-ray bursts, the diurnal and seasonal variations in these parameters are also observed. There have been a number of studies investigating the diurnal and seasonal variability of the SR parameters [e.g., *Balser and Wagner*, 1962; *Galejs*, 1972; *Sentman and Fraser*, 1991; *Sátori*, 1996]. The simultaneous measurements in California and Australia reported by *Sentman and Fraser* [1991] show a clear modulation in SR power related to local ionospheric height. *Price and Melnikov* [2004] reported the diurnal and seasonal variations in three main SR parameters (power, frequency, Q factor) on the basis of a 4-year measurement. Three dominant power maxima have been found in the diurnal cycle corresponding to the lightning activity in Southeast Asia, Africa and South America. The authors concluded that the global lightning

[1]Communications and Space Sciences Laboratory, Pennsylvania State University, University Park, Pennsylvania, USA.

0048-6604/06/2005RS003402$11.00

activity is an important factor to affect the SR power variation, besides the day-night asymmetry. Although, the frequency and Q factor variations reported by *Price and Melnikov* [2004] are too complicated to be easily interpreted, the frequency variation is in excellent agreement with the measurement reported by *Sátori* [1996]. Analysis of the SR observations at different stations reported by *Melnikov et al.* [2004] shows that there are obvious effects on SR parameters due to the day-night terminator and due to the relative positions of the observing stations with respect to lightning sources.

[5] In this paper, the diurnal and seasonal variation patterns of the power and frequency of the first SR mode are discussed and interpreted by comparing FDTD model results with realistic measurement data reported by *Price and Melnikov* [2004]. We also discuss the effects of the global lightning activity, local time, and relative position of the observation point with respect to the main lightning centers on the SR parameter variations.

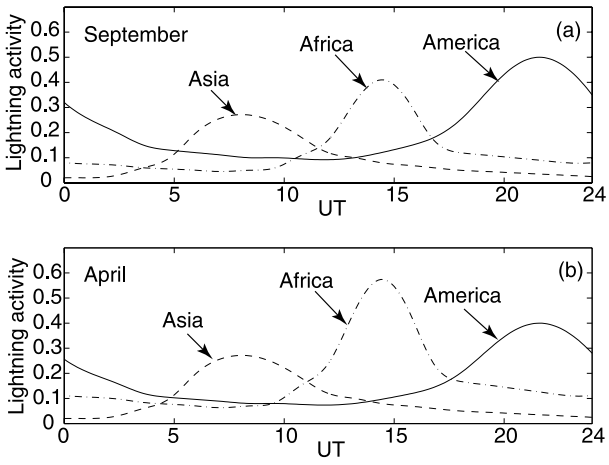

Figure 1. Diurnal variation of the average lightning activity in Southeast Asia, Africa, and South America in (a) September and (b) April [*Sentman and Fraser*, 1991].

2. Model Formulation

2.1. Three-Dimensional FDTD Modeling of Earth-Ionosphere Cavity

[6] We employ a three-dimensional FDTD model, which has been successfully applied to the studies of the SR frequency shifts during solar proton events and X-ray bursts in our previous work [*Yang and Pasko*, 2005]. In the present studies, the FDTD grid sizes in r, θ and ϕ directions near the equator are approximately 5, 1000 and 1000 km, respectively. The cavity is excited by a vertical lightning current with 5 km length, which has a linear risetime 500 μs and exponential fall with timescale 5 ms. The reported results for frequencies <40 Hz are not sensitive to the specifics of the chosen lightning current waveform. Prony's method [*Hildebrand*, 1956, p. 379; *Füllekrug*, 1995] is employed to find the slight SR frequency shifts by fitting the time domain data with complex polynomials.

2.2. Global Lightning Activity in Earth-Ionosphere Cavity

[7] In the Earth-ionosphere cavity, the lightning activity mainly concentrates in three major areas: Southeast Asia, Africa and South America. The magnitude of the lightning activity in these three regions reaches the peak at different time in the diurnal cycle [*Sentman*, 1995].

[8] Figure 1 indicates the diurnal variation of the global lightning activity in the three major lightning regions [*Sentman and Fraser*, 1991]. The total lightning activity in Southeast Asia, Africa, and South America reaches maximum at approximately 0800, 1400, and 2200 UT, respectively. Moreover, the maximum magnitude of the lightning activity varies with seasons. In September, the lightning activity in the South America is stronger than that in Africa. In April, the lightning activity increases by 40% in Africa, and reduces by 20% in South America. The lightning activity in Southeast Asia remains approximately the same during these two seasons. In our simulations, the power and frequency of the first SR mode are calculated every 1.2 hour from 0000 to 2400 UT. Three simulations are performed at each specific time point. In each simulation, it is assumed that the lightning discharges are uniformly distributed in a rectangular region centered at 27°E, 9°S; 99°E, 9°S; and 63°W, 9°S, corresponding to the three main lightning regions at Africa, Southeast Asia and South America, respectively, and the size of this source region is 3 cells × 3 cells (i.e., about 3000 km × 3000 km). The magnitude of each source at three major lightning regions was modulated as a function of time to reflect the lightning activity variation shown in Figure 1. Since the Earth-ionosphere cavity can be considered as a linear system, we can deal with these three sources separately. The total signal used in the final analysis can be expressed by the sum of the waves from these three sources. The modeling receiver is located at $\theta = 63°$ and $\phi = 36°$ just above the ground corresponding to the realistic location of the SR field station (35.45°E, 30.35°N) near the town of Mitzpe Ramon, in the Negev desert, Israel [*Price and Melnikov*, 2004]. The vertical electrical field component (E_r) and magnetic components in east-west (H_{EW}) and north-south (H_{NS}) direction are calculated and compared with measurements reported by *Price and Melnikov* [2004].

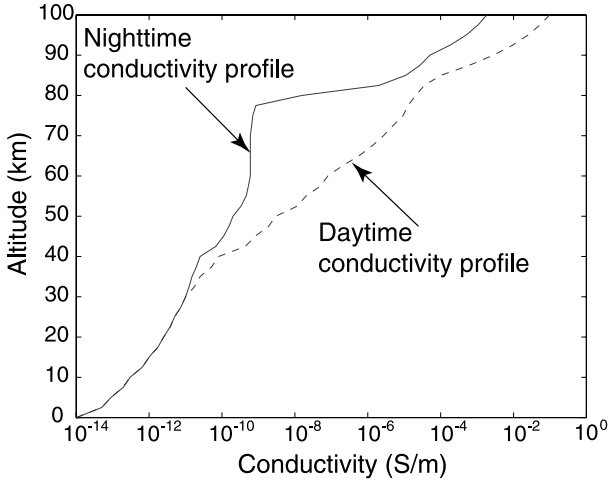

Figure 2. Conductivity profiles at daytime and nighttime in the Earth-ionosphere cavity.

2.3. Conductivity Profile in the Earth-Ionosphere Cavity

[9] The SR parameters are sensitive to the electromagnetic properties of the Earth-ionosphere cavity, which are mainly determined by the conductivity distribution in the cavity. Therefore the vertical conductivity profile at different locations around the globe plays a very important role in the SR research. Some conductivity models, e.g., two–scale height profile [*Sentman*, 1990, 1996] and "knee" model [*Mushtak and Williams*, 2002], have been developed to account for the conductivity distribution in the lower ionosphere. The SR parameters derived from these two models are very close to the realistic measurements [e.g., see *Mushtak and Williams*, 2002, Table 4]. However, these two models are spherically uniform, in contrast to the realistic cavity with day-night asymmetry due to the solar radiation. To account for the realistic conductivity distribution in the Earth-ionosphere cavity, the conductivity profiles used in this paper are derived from International Reference Ionosphere (IRI) model [*Bilitza*, 2001].

[10] Figure 2 illustrates two representative night and day time total conductivity profiles used in calculations. The profiles in Figure 2 are collected at 0000 UT, on 15 September 2000, at 0°E, 0°N and 180°E, 0°N, respectively. At altitude <60 km, the total conductivity is dominated by the ion conductivity, σ_i. The ion conductivity profile is taken from *Hale* [1984] and *Huang et al.* [1999]. Above 60 km, the electron conductivity σ_e is dominant over the ion conductivity, and can be determined by $\sigma_e = N_e q_e \mu_e$ where q_e is the charge of the electron, N_e is the IRI defined electron number density, μ_e is the mobility of the electrons given by $\mu_e = 1.36 N_0 / N \frac{m^2}{Vs}$, where $N_0 = 2.688 \times 10^{25}\ m^{-3}$, and N is altitude-dependent number density of air molecules [*Pasko et al.*, 1997]. The electron density in the cavity, N_e, is derived from the IRI model on 15 April 2000 and 15 September 2000 from 0000 to 2400 UT to account for the diurnal electron density variation during the Spring and Fall seasons, respectively. The total conductivity σ is derived as $\sigma = \sigma_i + \sigma_e$.

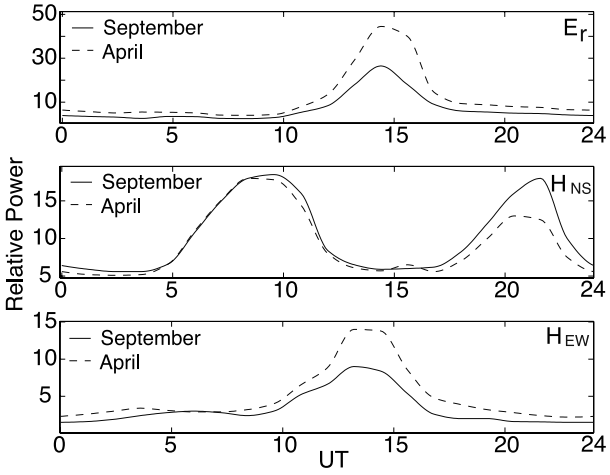

Figure 3. Diurnal power variations in the E_r, H_{NS}, and H_{EW} components.

3. Results

[11] Figures 3 and 4 report FDTD results and realistic measurements taken from a 4-year measurement [*Price*

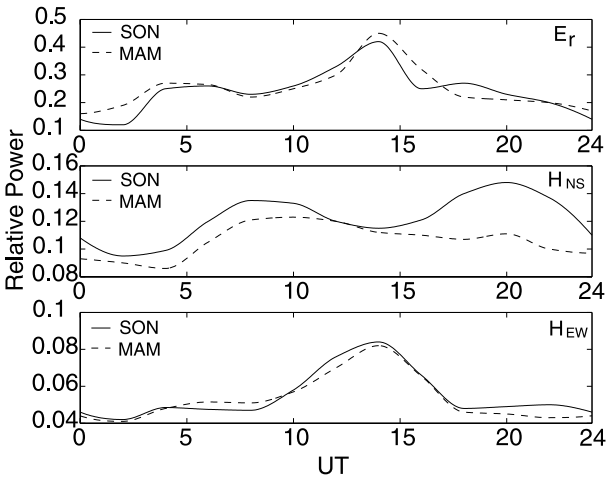

Figure 4. Realistic diurnal power variations in the E_r, H_{NS}, and H_{EW} components measured by *Price and Melnikov* [2004]. The abbreviations SON and MAM correspond to periods of time from September to November and from March to May, respectively.

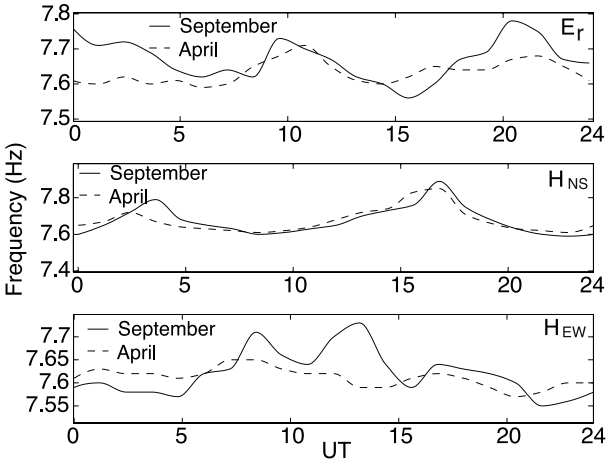

Figure 5. Diurnal frequency variations in the E_r, H_{NS}, and H_{EW} components.

and Melnikov, 2004] on the power variations in the E_r, H_{EW}, and H_{NS} components of the first SR mode as a function of universal time, and Figures 5 and 6 illustrate the diurnal frequency variations of these components, which are derived from our FDTD model and taken from [*Price and Melnikov*, 2004], respectively.

[12] The solid and dashed lines in Figure 3 describe the SR power variations in September and April, respectively. The variation patterns of the E_r and H_{EW} components have similar shape. The power begins increasing around 0500 UT, and a stronger power peak is found at 1400 UT in both cases. In addition, the peak in April at 1400 UT is stronger than that in September. For the H_{NS} component, a different variation pattern is observed. The power reaches its peaks around 0800 and 2200 UT. The power magnitude at 2200 UT in April is weaker than that in September, and remains approximately same at 0800 UT. All of these features are in good agreement with the realistic measurements reported by *Price and Melnikov* [2004] shown in Figure 4.

[13] In Figure 5, the first mode SR frequency of the E_r component has a maximum at 1000 and 2200 UT ranging from 7.6 to 7.8 Hz. For the H_{EW} component, the frequency ranges from 7.6 to 7.8 Hz, and two peaks appear around 0300 and 1600 UT, both in September and April. Three peaks can be found in the H_{NS} component around 0800, 1200, and 1600 UT. By comparing with the realistic measurements reported by *Price and Melnikov.* [2004] and shown in Figure 6, some similar features are found. For the E_r component, a frequency peak appearing around 1000 UT is close to the FDTD result, which also shows a peak appearing at this time. In addition, the peak around 0300 UT in the H_{NS} also matches the features appearing in the FDTD results. However, we emphasize that the agreement is not as good as in the case of the power variation.

4. Discussion

4.1. Power Variation

[14] *Price and Melnikov* [2004] have recently reported the diurnal and seasonal variations of the frequency and power of the first SR mode. A good agreement is found between our FDTD results and the realistic measurements of the first SR mode power variation. As shown in Figure 3, the power variations of the E_r and H_{EW} have same patterns, which have two peaks at 0500 and 1400 UT, respectively. The peak at 0500 UT can be explained by day-night terminator effect. Because the receiver is located at 36.0°E, 27.0°N, the sunrise time at that location is approximately at 0400 UT. During sunrise, the ionospheric boundary moves downward because of the solar radiation. Therefore a corresponding increase in the SR power starting from 0400 UT is observed in Figure 3 and reaches its peak at 0500 UT. The second peak in the E_r and H_{EW} components at 1400 UT is much stronger than that at 0500 UT, because the lightning activity in the Africa reaches its maximum around 1400 UT. The power variation in the H_{NS} component undergoes different variation pattern in comparison with other two components (Figure 3). Two peaks associated with the lightning activity from Southeast Asia and South America are found around 0900 and 2200 UT. The seasonal power variation is also obviously observed in Figure 3. It is believed that this seasonal variation is related to the seasonal variation of global lighting activity. In April, the lightning activity in Africa

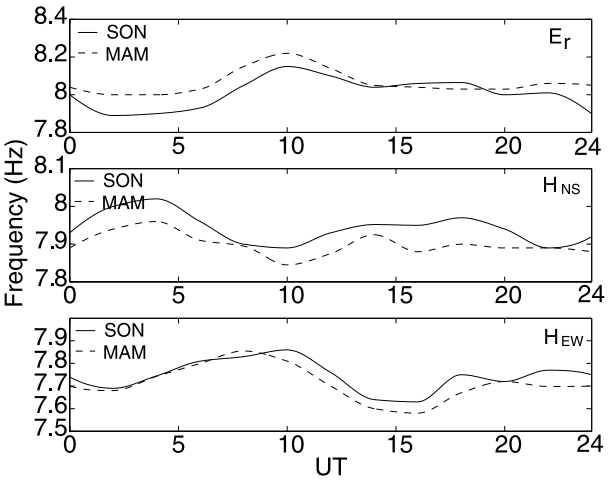

Figure 6. Realistic diurnal frequency variations in the E_r, H_{NS}, and H_{EW} components measured by *Price and Melnikov* [2004].

is stronger than that in September (see Figure 1). Therefore the corresponding SR power increases in the E_r and H_{EW} components around 1500 UT in April are observed. Since the magnitude of the lightning activity in Southeast Asia employed in this paper remains approximately the same in April and September, there is no obvious difference in the SR power at 0900 UT in the H_{NS} component for both seasons. The SR power peak at 2200 UT is stronger in September because of the stronger lightning activity in South America in September. *Price and Melnikov* [2004] report that the magnitude of SR power at 1400 UT from September to November (SON) is a little stronger than that from March to May (MAM) in the E_r component, and remains approximately same in SON and MAM in H_{EW} components. The two peaks in the H_{NS} component around 0800 and 2000 UT in SON are stronger than these in MAM.

[15] The differences observed between experimental data and FDTD results may be related to fine details of global lightning activity as a function of time employed in FDTD model. The FDTD results are derived from two profiles of global lightning activity (see Figure 1) on the basis of 24-hour averages during 14–21 April 1990 and 2–17 September 1989, respectively [*Sentman and Fraser*, 1991], while the realistic data [*Price and Melnikov*, 2004] are based on a 4-year measurement (1999–2003). We can imply from the data presented by *Price and Melnikov* [2004] that the average magnitude of the lightning activity in Africa from 1999 to 2003 remained approximately the same in MAM and SON, and in Southeast Asia and South America, the magnitude of global lightning in SON was stronger than that in MAM.

[16] In addition, the relative positions of the three main lightning regions with respect to the receiver also have effects on the power variation in E_r, H_{NS}, and H_{EW} components. The source accounting for the lightning activity in Africa is located at 27°E, and is very close to the receiver located at 36°E. Therefore the H field from Africa collected by the receiver is dominated by the east-west component. Meanwhile, the H fields excited by the lightning at Southeast Asia and South America are preferentially in the north-south direction because of the relative positions of the source with respect to the receiver. Therefore two peaks are observed at 0800 and 2200 UT in the H_{NS} component corresponding to the lightning activity peaks in these two regions and a peak associated with the lightning activity in Africa is clearly found at 1500 UT in the H_{EW} component. For the first SR mode, a null of E_r component appears at the distance of approximately 10000 km from the source. The sources at Southeast Asia and South America are approximately 8000 km and 11000 km away from the receiver. Because of the null proximity, these two sources contribute much less to the E_r component at the receiver than that at Africa, which is only 3000 km from the receiver. Therefore only the peak around 15:00 in E_r component is obviously observed.

[17] *Melnikov et al.* [2004] reported a terminator effect on Schumann resonances. Here, we employ our FDTD model to describe this effect. Twenty simulations have been performed to calculate the variation of the distribution of the magnitude of the E_r component of the first SR mode in the cavity due to the day-night terminator position during a diurnal cycle. The conductivity profiles used in these simulations are the same as we used to obtain the results reported in Figure 3. For illustrative purposes, only one source with the same magnitude is used, which is located at 0°E 0°N, and 40 receivers are positioned on the Earth surface at equal intervals along the equator. Figures 7, 8, 9, and 10 show the variation of the E_r distribution of the first SR mode during the 0000 to 2400 UT time interval. The dashed line depicts the position of the day-night terminator at different instants of time. The letters "D" and "N" in the figures mark the day and night regions, respectively. From these 20 plots, it can be seen that the magnitude of the first SR mode is generally stronger during daytime in comparison with nighttime at a fixed position. For example, at longitude 30°, the magnitude of the E_r component increases during sunrise, and decreases during sunset, which agrees with what has been previously reported by *Melnikov et al.* [2004]. This variation can be associated with the variation of the ionospheric height. The magnitude of the E_r component during daytime is approximately 60% stronger than that during nighttime. We also find that the SR magnitude is stronger when the source is near the day-night terminator (see plots corresponding to 0600 and 1800 UT) than at other times. However, in our FDTD model, we find that the power variations of the first SR mode during the sunrise and sunset are much smaller than those associated with the peaks of the global lightning activity (see Figure 3). This difference can be explained by the different sources used in these two simulations. In Figures 7–10, only one source with constant magnitude is employed. In Figure 3, many sources with different magnitude are used to account for the diurnal variations of the lightning activity at three lightning centers (as described in section 2.2), and the results are in good agreement with the realistic measurements [*Price and Melnikov*, 2004]. Therefore we believe that the global lightning activity plays a more important role in the variations of the SR power.

[18] The effect of the local time in the SR power is well known. According to *Sentman and Fraser* [1991] and *Melnikov et al.* [2004], it can be explained by the variation of the altitude of the ionospheric boundary over an observation point due to solar radiation. Meanwhile, the sources of SR, global lightning activity, tending to maximize at specific universal time in three main lightning regions in a diurnal cycle lead to a corresponding

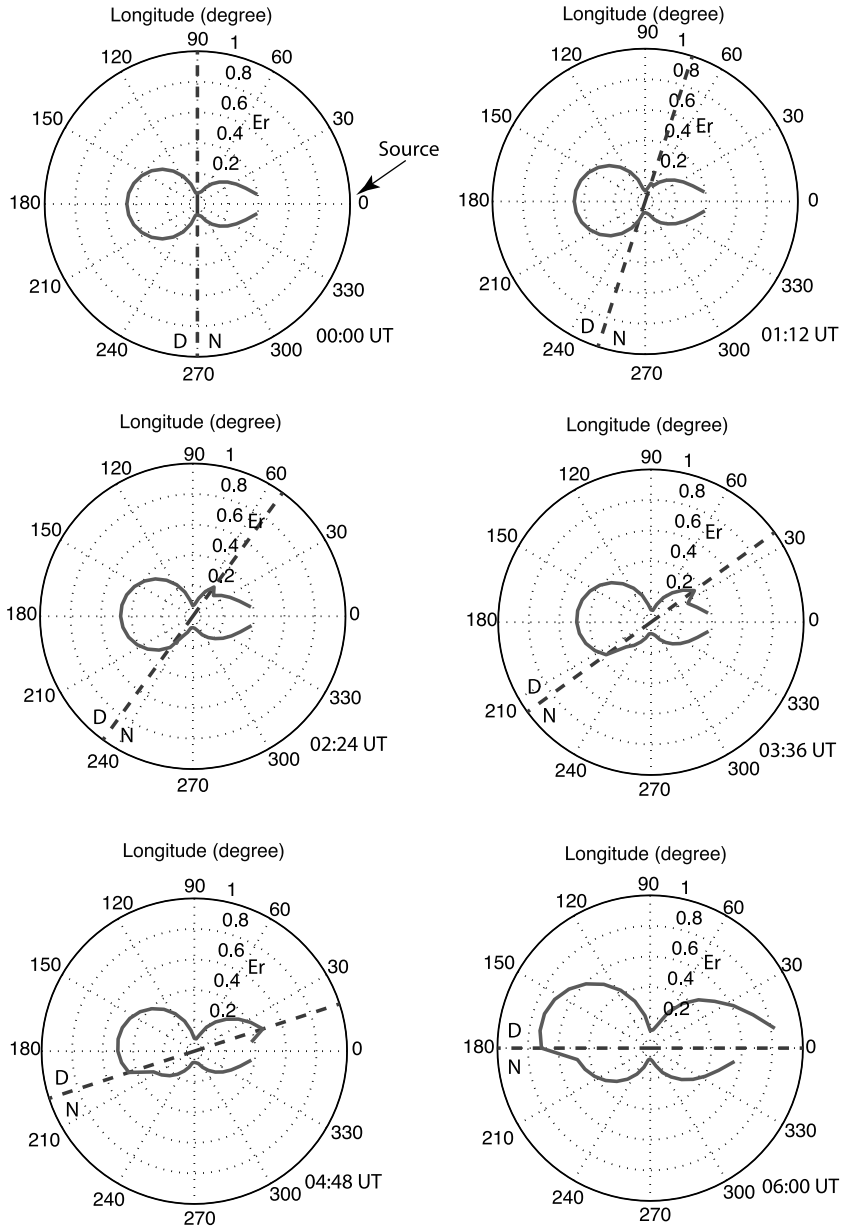

Figure 7. Magnitude of the E_r component of the electric fields on the surface of the Earth at the equator as a function of longitude. The six plots correspond to different instants of time during the diurnal cycle between 0000 and 0600 UT.

intensification of SR power. Therefore it is believed that the universal time also plays an important role in the variations of SR power. In addition as discussed above, the SR power variations are also influenced by the relative position of the observation point with respect to the main lightning centers, due to the field distribution of SR around the source and the wave orientation.

4.2. Frequency Variation

[19] The variation of SR frequencies can be explained by mode splitting theory presented by *Sentman* [1989] due to the asymmetry in the Earth-ionosphere cavity at the day and night sides. The magnitude of the line splitting is in the range of 1.4–1.8 Hz for the cases studied by *Sentman* [1989]. Because of the strong damp-

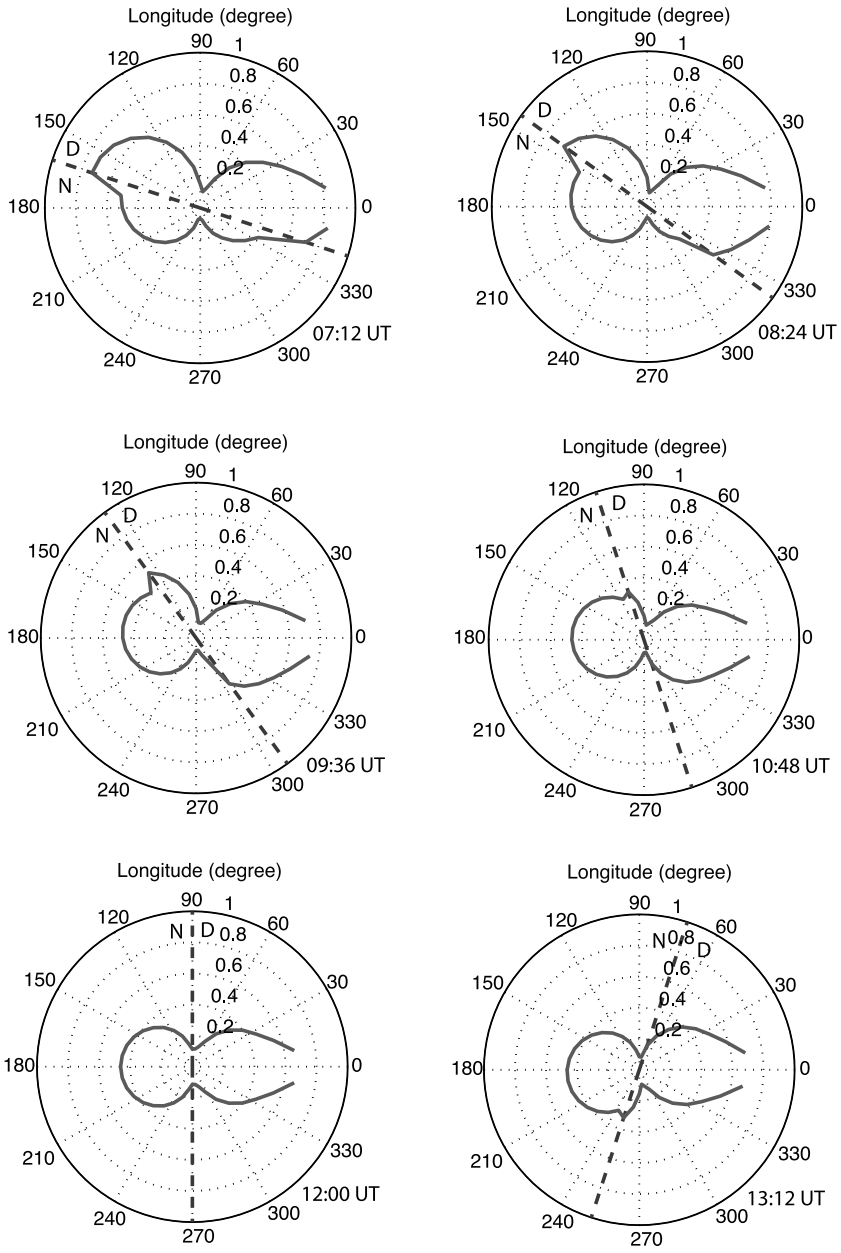

Figure 8. Same as Figure 7 but for time period 0712 to 1312 UT.

ing in the Earth-ionosphere cavity, the magnitude of the mode splitting is less than or comparable to the inherent width of the lines themselves [*Sentman*, 1989], which complicates the determination of the eigenfrequencies of the cavity.

[20] Comparing our FDTD results and data reported by *Price and Melnikov* [2004], some different features are observed in these two frequency variation patterns (see Figures 4 and 6 and section 3). One of the reasons for this difference may be related to the fact that the frequency variations are averaged over 3 months in the work by *Price and Melnikov* [2004], while the FDTD results are derived from a model with conductivity profiles corresponding to 15 September 2000 and 15 April 2000. Therefore the difference between these two results can be expected. Another possible reason for

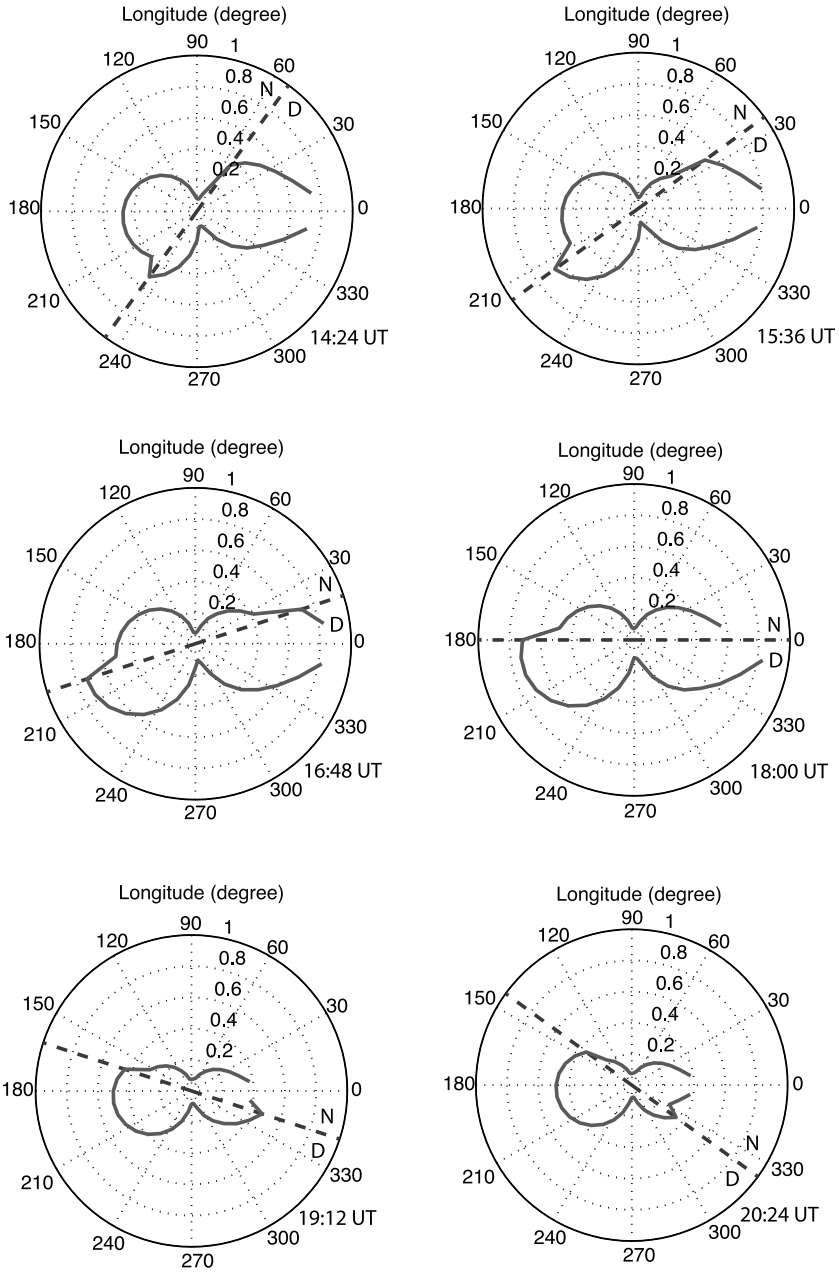

Figure 9. Same as Figure 7 but for time period 1424 to 2024 UT.

this difference is the different methods employed to find the eigenfrequencies. *Price and Melnikov* [2004] used a Lorentzian function fitting method to derive the eigenfrequencies of the cavity, assuming that there is only one frequency component in each resonance mode. The Lorentzian fitting method is generally suitable for the application in uniform cavity without mode splitting, and an example is presented in our previous work [*Yang and Pasko*, 2005; *Yang et al.*, 2006]. *Sentman* [1989] found the maximum magnitude of the first mode splitting to be in the range 1.4–1.8 Hz in realistic measurements. If only one frequency component is used to fit all of the splitting modes, the result will be influenced by the magnitude of all of the splitting modes, and the maximum error can be

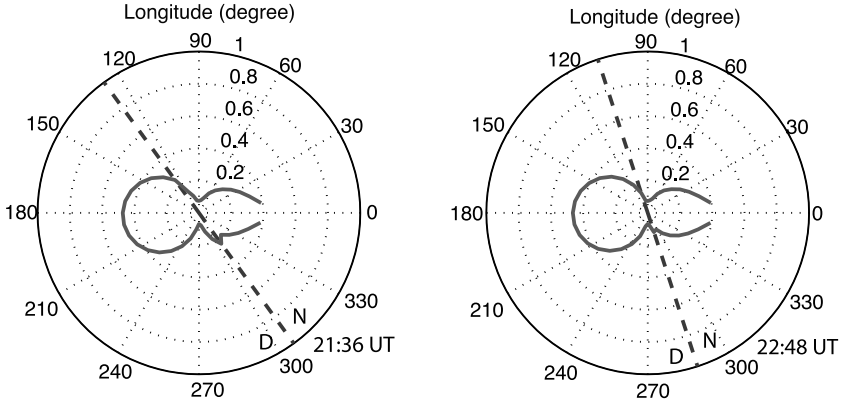

Figure 10. Same as Figure 7 but for time period 2136 to 2248 UT.

half splitting range (0.7–0.9 Hz), which can mask the real variation of the resonance frequency. Therefore the Lorentzian function fitting method is not applicable as an accurate method to find the eigenfrequencies of the realistic cavity with mode splitting. In this paper, Prony's method is employed to find the eigenfrequencies of the cavity, by which the mode splitting can be clearly detected. Figure 11 shows the comparison of these two methods for analysis of the H_{EW} component derived from the FDTD model with conductivity profile at 0840 UT on 15 September 2000. The result derived from Prony's method matches the original power spectrum data (solid line in Figure 11) much better than that from the Lorentzian function fitting method (dashed line in Figure 11). By the Lorentzian function fitting method, the first SR frequency is found at 7.45 Hz. By Prony's method, the first SR mode can be found splitting into 7.7 Hz and 7.59 Hz. Because the magnitude of 7.7 Hz mode is much stronger than that of 7.59 Hz mode, we used 7.7 Hz as the first SR frequency to show results presented in Figure 5. A 0.25 Hz difference can be found between these two methods and this difference is close to the magnitude of frequency variations reported by *Price and Melnikov* [2004].

[21] *Roldugin et al.* [2004b] concluded that diurnal SR frequency variation is mainly controlled by local time, and the different field components undergo different variation patterns because of the horizontal inhomogeneity of the ionosphere. *Nickolaenko et al.* [1998] found that the source area of the global lightning activity also plays an important role affecting the SR frequency variation. We conducted additional simulations (not shown), in which we changed the magnitude of the lightning activity at the three lightning centers, as well as the area and positions of these three lightning centers. We observed the obvious changes of the frequency variation pattern. At a specific time, the mode splitting produced by all of the lightning activity in the cavity is determined by the magnitude of each of the lightning discharges, and their positions with respect to the day-night terminator. With changing the area and the positions of these lightning centers, which determine the positions of the lightning discharges in these centers with respect to the day-night terminator, and the magnitude of these lightning centers, the associated change of the mode splitting leading to the SR frequency variation is expected. Therefore we conclude that the magnitude of the lightning activity in three lightning centers, as well as the area and positions of these three lightning centers are the three main factors controlling the SR frequency variation.

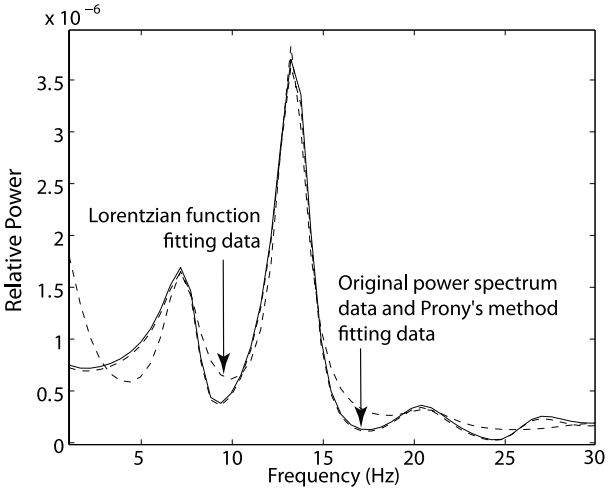

Figure 11. Comparison of Prony's method and the Lorentzian function fitting method.

[22] **Acknowledgments.** This research was supported by NSF ATM-0134838 grant to Penn State University. The authors thank Gabriella Sátori for useful discussions related to the connections between the area of the lightning centers and the SR frequency variation.

References

Balser, M., and C. A. Wagner (1962), On frequency variations of the Earth-ionosphere cavity mode, *J. Geophys. Res.*, *67*, 4081.

Bilitza, D. (2001), International Reference Ionosphere 2000, *Radio Sci.*, *36*(2), 261.

Cummer, S. A. (2000), Modeling electromagnetic propagation in the Earth-ionosphere waveguide, *IEEE Trans. Antennas Propag.*, *4*(9), 1420.

Füllekrug, M. (1995), Schumann-resonances in magnetic-field components, *J. Atmos. Terr. Phys.*, *57*, 479.

Hale, L. C. (1984), Middle atmosphere electrical structure, dynamics, and coupling, *Adv. Space Res.*, *4*, 175.

Hildebrand, F. B. (1956), *Introduction to Numerical Analysis*, McGraw-Hill, New York.

Huang, E., E. Williams, R. Boldi, S. Heckman, W. Lyons, M. Taylor, T. Nelson, and C. Wong (1999), Criteria for sprites and elves based on Schumann resonance observation, *J. Geophys. Res.*, *104*, 16,943.

Galejs, J. (1972), *Terrestrial Propagation of Long Electromagnetic Waves*, Elsevier, New York.

Melnikov, A., C. Price, G. Sátori, and M. Füllekrug (2004), Influence of solar terminator passages on Schumann resonance parameters, *J. Atmos. Sol. Terr. Phys.*, *66*, 1187.

Mushtak, V. C., and E. Williams (2002), ELF propagation parameters for uniform models of the Earth-ionosphere waveguide, *J. Atmos. Sol. Terr. Phys.*, *64*, 1989.

Nickolaenko, A. P, M. and Hayakawa (2002), *Resonances in the Earth-Ionosphere Cavity*, Springer, New York.

Nickolaenko, A. P., G. Sátori, B. Zieger, L. M. Rabinowicz, and I. G. Kuduntseva (1998), Parameters of global thunderstorm activity deduced from the long-term Schumann resonance records, *J. Atmos. Sol. Terr. Phys.*, *60*, 387.

Pasko, V. P., U. S. Inan, T. F. Bell, and Y. N. Taranenko (1997), Sprites produced by quasi-electrostatic heating and ionization in the lower ionosphere, *J. Geophys. Res.*, *102*(A3), 4529.

Price, C., and A. Melnikov (2004), Diurnal, seasonal and interannual variations of the Schumann resonance parameters, *J. Atmos. Sol. Terr. Phys.*, *66*, 1179.

Roldugin, V. C., Y. P. Maltsev, G. A. Petrova, and A. N. Vasiljev (2001), Decrease of the first Schumann resonance frequency during solar proton events, *J. Geophys. Res.*, *106*, 18,555.

Roldugin, V. C., Y. P. Maltsev, A. N. Vasiljev, A. V. Shvets, and A. P. Nikolaenko (2003), Changes of Schumann resonance parameters during the solar proton event of 14 July 2000, *J. Geophys. Res.*, *108*(A3), 1103, doi:10.1029/2002JA009495.

Roldugin, V. C., Y. P. Maltsev, A. N. Vasiljev, A. Y. Schokotov, and G. G. Belyajev (2004a), Schumann resonance frequency increase during solar X-ray bursts, *J. Geophys. Res.*, 109, A01216, doi:10.1029/2003JA010019.

Roldugin, V. C., Y. P. Maltsev, A. N. Vasiljev, A. Y. Schokotov, and G. G. Belyajev (2004b), Diurnal variations of Schumann resonance frequency in NS and EW magnetic components, *J. Geophys. Res.*, *109*, A08304, doi:10.1029/2004JA010487.

Sátori, G. (1996), Monitoring Schumann resonances—II. Daily and seasonal frequency variations, *J. Atmos. Terr. Phys.*, *58*, 1483.

Sátori, G., E. Williams, and V. Mushtak (2005), Response of the Earth-ionosphere cavity resonator to the 11-year solar cycle in X-radiation, *J. Atmos. Sol. Terr. Phys.*, *67*, 553.

Schlegel, K., and M. Füllekrug (1999), Schumann resonance parameter changes during high-energy particle precipitation, *J. Geophys. Res.*, *104*, 10,111.

Schumann, W. O. (1952), Uber die strahlungslosen einer leitenden Kugel die von einer Luftschicht und einer Ionosphareenhulle umgeben ist, *Z. Naturforsch. A*, *7*, 149.

Sentman, D. D. (1989), Detection of elliptical polarization and mode splitting in discrete Schumann resonance excitations, *J. Atmos. Terr. Phys.*, *51*, 507.

Sentman, D. D. (1990), Approximate Schumann resonance parameters for a 2-scale-height ionosphere, *J. Atmos. Terr. Phys.*, *52*, 35.

Sentman, D. D. (1995), Schumann resonances, in *Handbook of Atomospheric Electrodynamics*, edited by H. Volland, p. 267, CRC Press, Boca Raton, Fla.

Sentman, D. D. (1996), Schumann resonance spectra in a two-scale-height Earth-ionosphere cavity, *J. Geophys. Res.*, *101*, 9479.

Sentman, D. D., and B. J. Fraser (1991), Simultaneous observations of Schumann resonances in California and Australia: Evidence for intensity modulation by the local height of the D-region, *J. Geophys. Res.*, *96*, 15,973.

Shvets, A. V. (2001), A technique for reconstruction of global lightning distance profile from background Schumann resonance signal, *J. Atmos. Sol. Terr. Phys.*, *63*, 1061.

Williams, E. R. (1992), The Schumann resonance—A global tropical thermometer, *Science*, *256*(5060), 1184.

Yang, H., and V. P. Pasko (2005), Three-dimensional finite difference time domain modeling of the Earth-ionosphere cavity resonances, *Geophys. Res. Lett.*, 32, L03114, doi:10.1029/2004GL021343.

Yang, H., V. P. Pasko, and Y. Yair (2006), Three-dimensional finite difference time domain modeling of the Schumann resonance parameters on Titan, Venus, and Mars, *Radio Sci.*, 41, RS2S03, doi:10.1029/2005RS003431.

V. P. Pasko and H. Yang, CSSL, Pennsylvania State University, 211B EE East, University Park, PA 16802, USA. (vpasko@psu.edu; hxy149@psu.edu)